6

SPIN WAVES IN PERIODIC STRUCTURES

Because of the modification of the translational symmetry, the spin waves in modulated magnetic structures display certain interesting aspects which are not shared by the simple ferromagnetic structure. However, this same feature makes their experimental study considerably more difficult, and the results which have been obtained on such systems are still relatively sparse. This chapter is correspondingly short, and in its two sections we distinguish between structures *incommensurable* with the lattice periodicity, when the translational symmetry in the direction of the wave-vector is, in principle, destroyed, and *commensurable* structures, in which this symmetry is only modified, though possibly quite drastically.

The stringent mathematical definition of an incommensurable structure is straightforward, but it presupposes that the coherence lengths of the lattice and of the magnetic system are both infinite. In this idealized case, an irrational ratio between the periodicities of the two subsystems breaks the translational invariance, the wave-vector $\mathbf{q}$ is consequently no longer a good quantum number, and neutron-diffraction peaks acquire a non-zero width. Furthermore, the energy eigenvalues which determine the excitation spectrum also have a certain width when projected on to $\mathbf{q}$-space, which is the appropriate representation for interpreting constant-$\mathbf{q}$ neutron-scattering experiments. The alternative method of distinguishing experimentally between the two types of structure is to follow the ratio between the two periodicities as a function of temperature or external field. If this ratio changes *discontinuously* between constant steps, the structure is commensurable. On the other hand, if the variation is observed to be *continuous*, the structure is usually classified as being incommensurable. As examples of transverse incommensurable structures, we shall accordingly take the *helix* in Tb, which exists only over a small range of temperature below T_N, and the low-temperature *cone* in Er. It is generally questionable whether any particular structure can strictly be classified as incommensurable but, as we shall see, the distinction in these cases is unimportant. The magnetic high-temperature phase of Er is treated as an example of an incommensurable *longitudinal-wave structure*, although it may only be truly incommensurable at the highest temperatures in the ordered phase. In

this case, the incommensurability has significant qualitative effects on the excitation spectrum.

In a commensurable structure, where $m|\mathbf{Q}| = mQ_c$ is p times the length $4\pi/c$ of the (effective) reciprocal lattice vector, the number m of layers between magnetically-identical lattice planes will have an important influence on the character of the excitations. If m is small, they will be well-defined, long-lived at low temperatures, and relatively easy to study experimentally. As examples of such ideal commensurable structures, we shall consider the low-temperature *bunched helix* in Ho, and the *longitudinal ferrimagnetic structure* in Tm, where the crystal fields make a decisive contribution. These relatively simple structures are stable at low temperatures but, in both cases, the configuration of the moments becomes more complicated as the temperature is increased. In Ho, for example, *spin-slip structures* of reduced symmetry and generally increasing m evolve, and the excitations, of which only preliminary studies have so far been made, become correspondingly complex. Although these excitations may be just as well-defined as when m is small, the extension of the magnetic Brillouin zone, in the c-direction, is reduced by the factor $1/m$, while the number of branches in the dispersion relation is multiplied by m. The different branches are separated from each other by energy gaps at the boundaries of the magnetic Brillouin zone, and the corresponding excitations scatter neutrons with different weight, depending on the scattering vector and described in terms of the *dynamical structure factor*. If m is large, however, it may be extremely difficult to resolve the different branches experimentally. As m increases towards the values of the order of 50 which characterize some of the commensurable structures presented in Section 2.3, imperfections in the lattice, or boundaries between different magnetic domains, become more important. We should also expect that disordering phase-slips would become relatively more frequent, leading to a less well-defined structure, and disturbing the very long-range periodicity. It is unlikely that a specific pattern involving 100 or more layers could be repeated many times in the crystal, without significant errors, and we might rather anticipate a somewhat chaotic arrangement, where the phase factor characterizing the moments changes systematically from layer to layer, but with an occasional minor phase slip, so that the structure never repeats itself exactly. This kind of structure may frequently in practice be described as incommensurable.

6.1 Incommensurable periodic structures

In this section, we shall first discuss the spin waves in the regular helix or cone, including the hexagonal anisotropy only as a minor perturbation. On account of the infinitely larger number of irrational than rational

numbers, these structures are most naturally classified as incommensurable, particularly as the distinction is immaterial in this case. If the hexagonal anisotropy and possible external fields are neglected, the translational symmetry is broken only formally, as a rigid rotation of the moments, or of the total system, around the spiral axis costs no energy. We then consider the longitudinally polarized phase, in which genuine effects due to incommensurability would be expected. On the other hand, the stronger coupling between the two periodicities increases the tendency of the magnetic-ordering wave-vector to lock into a value which is commensurable with the lattice. It may perhaps be questioned whether theoretical results derived for ideal incommensurable models are relevant to real, three-dimensional systems. However, it appears that the essential features of systems which are classified experimentally as incommensurable may be described theoretically as such, provided that the analysis includes an averaging or *coarse graining* of the results, of a magnitude somewhat smaller than the experimental resolution.

6.1.1 The helix and the cone

A helical ordering of the moments in an hcp lattice, with a wave-vector $\mathbf{Q}$ along the c- or ζ-axis, is described by the following equations:

$$\begin{aligned} \langle J_{i\xi} \rangle &= \langle J_\perp \rangle \cos\left(\mathbf{Q}\cdot\mathbf{R}_i + \varphi\right) \\ \langle J_{i\eta} \rangle &= \langle J_\perp \rangle \sin\left(\mathbf{Q}\cdot\mathbf{R}_i + \varphi\right) \\ \langle J_{i\zeta} \rangle &= 0. \end{aligned} \tag{6.1.1}$$

As usual, we shall be most interested in excitations propagating in the c-direction, and hence may use the double-zone representation, corresponding to the case of a Bravais lattice. The moments of constant length $\langle J_\perp \rangle$ lie in the ξ–η plane perpendicular to $\mathbf{Q}$, and rotate uniformly in a right-handed screw along the $\mathbf{Q}$-vector. The elastic cross-section corresponding to this structure is, according to (4.2.6),

$$\begin{aligned} \frac{d\sigma}{d\Omega} = N\left(\frac{\hbar\gamma e^2}{mc^2}\right)^2 e^{-2W(\kappa)} |\tfrac{1}{2} g F(\boldsymbol{\kappa})|^2 \langle J_\perp \rangle^2 (1+\hat{\kappa}_\zeta^2) \\ \times \frac{(2\pi)^3}{v} \sum_\tau \frac{1}{4} \left\{ \delta(\boldsymbol{\tau} + \mathbf{Q} - \boldsymbol{\kappa}) + \delta(\boldsymbol{\tau} - \mathbf{Q} - \boldsymbol{\kappa}) \right\}. \end{aligned} \tag{6.1.2}$$

In this system the molecular field in (3.5.3) changes from site to site, as does the MF susceptibility $\overline{\overline{\chi}}_i^{\,o}(\omega)$ in (3.5.7). This complication may be alleviated by transforming into a rotating (xyz)-coordinate system with the z-axis parallel to the moments, i.e.

$$\begin{aligned} J_{i\xi} &= J_{iz}\cos\phi_i + J_{iy}\sin\phi_i \\ J_{i\eta} &= J_{iz}\sin\phi_i - J_{iy}\cos\phi_i \\ J_{i\zeta} &= J_{ix}, \end{aligned} \tag{6.1.3}$$

where $\phi_i = \mathbf{Q}\cdot\mathbf{R}_i + \varphi$. Carrying out this transformation, we find that $\mathbf{J}_i\cdot\mathbf{J}_j$ becomes

$$(J_{iz}J_{jz} + J_{iy}J_{jy})\cos(\phi_i - \phi_j) + (J_{iy}J_{jz} - J_{iz}J_{jy})\sin(\phi_i - \phi_j) + J_{ix}J_{jx},$$

so that the Hamiltonian (3.5.1) may be written, in the (xyz)-coordinate system,

$$\mathcal{H} = \sum_i \mathcal{H}_{\mathrm{J}}(J_{ix}^2) - \frac{1}{2}\sum_{i\neq j}\sum_{\alpha\beta} J_{i\alpha}\mathcal{J}_{\alpha\beta}(ij)J_{j\beta}, \tag{6.1.4}$$

where α and β signify the Cartesian coordinates x, y, and z. Here we have assumed that the dependence of the single-ion anisotropy on $J_{i\xi}$ and $J_{i\eta}$ can be neglected, and that only even powers of $J_{i\zeta} = J_{ix}$ occur, since otherwise the helical structure becomes distorted and (6.1.1) is no longer the equilibrium configuration. The ordering wave-vector $\mathbf{Q}$ is determined by the minimum-energy condition that $\mathcal{J}(\mathbf{q})$ has its maximum value at $\mathbf{q} = \mathbf{Q}$. After this transformation, the MF Hamiltonian is the same for all sites:

$$\begin{aligned}\mathcal{H}_{\mathrm{MF}}(i) &= \mathcal{H}_{\mathrm{J}}(J_{ix}^2) - (J_{iz} - \tfrac{1}{2}\langle J_\perp\rangle)\sum_j \langle J_\perp\rangle\mathcal{J}(ij)\cos(\phi_i - \phi_j)\\ &= \mathcal{H}_{\mathrm{J}}(J_{ix}^2) - (J_{iz} - \tfrac{1}{2}\langle J_\perp\rangle)\langle J_\perp\rangle\mathcal{J}(\mathbf{Q}) \quad ; \quad \langle J_\perp\rangle = \langle J_z\rangle,\end{aligned} \tag{6.1.5}$$

as is the corresponding MF susceptibility $\overline{\overline{\chi}}^{\,o}(\omega)$. The price we have paid is that the two-ion coupling $\overline{\overline{\mathcal{J}}}(ij)$ is now anisotropic, and its non-zero Fourier components are

$$\begin{aligned}&\mathcal{J}_{xx}(\mathbf{q}) = \mathcal{J}(\mathbf{q}) \qquad ; \quad \mathcal{J}_{yy}(\mathbf{q}) = \mathcal{J}_{zz}(\mathbf{q}) = \frac{1}{2}\{\mathcal{J}(\mathbf{q}+\mathbf{Q}) + \mathcal{J}(\mathbf{q}-\mathbf{Q})\}\\ &\mathcal{J}_{yz}(\mathbf{q}) = -\mathcal{J}_{zy}(\mathbf{q}) = \frac{i}{2}\{\mathcal{J}(\mathbf{q}+\mathbf{Q}) - \mathcal{J}(\mathbf{q}-\mathbf{Q})\}.\end{aligned} \tag{6.1.6}$$

However, it is straightforward to take account of this complication in the RPA, and the result is the same as (3.5.8) or (3.5.21), with $\mathcal{J}(\mathbf{q})$ replaced by $\overline{\overline{\mathcal{J}}}(\mathbf{q})$,

$$\overline{\overline{\chi}}_t(\mathbf{q},\omega) = \left\{1 - \overline{\overline{\chi}}^{\,o}(\omega)\,\overline{\overline{\mathcal{J}}}(\mathbf{q})\right\}^{-1}\overline{\overline{\chi}}^{\,o}(\omega), \tag{6.1.7}$$

where the index t indicates that this is the (xyz)-susceptibility, and not the $(\xi\eta\zeta)$-susceptibility $\overline{\overline{\chi}}(\mathbf{q},\omega)$ which determines the scattering cross-section. From the transformation (6.1.3), it is straightforward, but somewhat cumbersome, to find the relation between the two susceptibility tensors.

In the general case, the MF susceptibility $\overline{\overline{\chi}}^{o}(\omega)$ is determined by three distinct diagonal components, plus the two off-diagonal terms $\chi^{o}_{xy}(\omega) = -\chi^{o}_{yx}(\omega)$, with the same analytical properties, (3.5.24*b*) and (5.2.42), as in the Heisenberg ferromagnet. It may be seen that $\chi^{o}_{xy}{}'(\omega)$, for instance, is imaginary by recalling that the MF Hamiltonian is independent of J_y, in which case the eigenvectors in the J_z-representation can all be chosen to be real, so that the products of the matrix elements of J_x and of J_y are imaginary. The vanishing of the other four off-diagonal terms follows from the two-fold symmetry about the z-axis of the MF Hamiltonian. In spite of this reduction, the analytical expression for $\overline{\overline{\chi}}(\mathbf{q},\omega)$ is still quite formidable. However, in most cases of interest, the single-ion anisotropy is relatively weak, and the inelastic modifications due to $\chi^{o}_{zz}(\omega)$ can be neglected, so that, for $\omega \neq 0$,

$$\begin{aligned}\chi_{xx}(\mathbf{q},\omega) &= \left\{\chi^{o}_{xx}(\omega) - |\,\overline{\overline{\chi}}^{o}(\omega)|\,\mathcal{J}_{yy}(\mathbf{q})\right\}/D(\mathbf{q},\omega)\\ \chi_{xy}(\mathbf{q},\omega) &= \left\{\chi^{o}_{xy}(\omega) + |\,\overline{\overline{\chi}}^{o}(\omega)|\,\mathcal{J}_{xy}(\mathbf{q})\right\}/D(\mathbf{q},\omega),\end{aligned} \tag{6.1.8a}$$

and the same relations hold with x and y interchanged. Here

$$D(\mathbf{q},\omega) = 1 - \sum_{\alpha\beta}\chi^{o}_{\alpha\beta}(\omega)\mathcal{J}_{\beta\alpha}(\mathbf{q}) + |\,\overline{\overline{\chi}}^{o}(\omega)|\,|\,\overline{\overline{\mathcal{J}}}(\mathbf{q})|, \tag{6.1.8b}$$

where α or β are x or y, and $|\,\overline{\overline{\chi}}^{o}(\omega)|$ or $|\,\overline{\overline{\mathcal{J}}}(\mathbf{q})|$ are the determinants of the 2×2 matrices. In the weak-anisotropy limit, we may to a good approximation use the result (5.2.42) derived in Section 5.2, and to first order in $1/J$, we have

$$\begin{aligned}\chi^{o}_{xx}(\omega) &= \langle J_z\rangle\frac{A - B + h_{\rm ex}}{E^2_{\rm ex} - (\hbar\omega)^2}\\ \chi^{o}_{yy}(\omega) &= \langle J_z\rangle\frac{A + B + h_{\rm ex}}{E^2_{\rm ex} - (\hbar\omega)^2}\\ \chi^{o}_{xy}(\omega) &= -\chi^{o}_{yx}(\omega) = \langle J_z\rangle\frac{i\,\hbar\omega}{E^2_{\rm ex} - (\hbar\omega)^2}\end{aligned} \tag{6.1.9a}$$

and $\chi^{o}_{zz}(\omega) \simeq \beta(\delta J_z)^2\,\delta_{\omega 0}$. The only modification is that the exchange field, given in eqn (6.1.5), is now

$$h_{\rm ex} = \langle J_z\rangle\mathcal{J}(\mathbf{Q}) \qquad \text{and} \quad E^2_{\rm ex} = (A + h_{\rm ex})^2 - B^2. \tag{6.1.9b}$$

There are inelastic contributions to $\chi^{o}_{zz}(\omega)$, but they are of the order $A/2JE_{\rm ex}$, relative to the other inelastic terms, and can be neglected.

The parameters A and B are the same as those derived in Section 5.2, when $\mathcal{H}_{\rm J}$ in (6.1.4) is replaced by the usual crystal-field Hamiltonian, except that we here neglect explicitly the hexagonal anisotropy

B_6^6. The result above may be generalized to include most of the renormalization effects appearing in the second order of $1/J$, by replacing $A \pm B$ by $A_{\mathbf{0}}(T) \pm B_{\mathbf{0}}(T)$, in accordance with the discussion at the end of Section 5.2. After the transformation to the rotating coordinates, the system becomes equivalent to the basal-plane ferromagnet, except that the hexagonal anisotropy is neglected and the γ-strains vanish, due to the lattice-clamping effect discussed in Section 2.2.2. Hence we may take $A \pm B$ to be $A_{\mathbf{0}}(T) \pm B_{\mathbf{0}}(T)$, given by eqn (5.3.22), with $B_6^6 = 0$ and $H = 0$.

In the present situation, where $\mathcal{H}_{\mathrm{J}}$ in (6.1.4) only depends on J_x^2, $A = B$ and (6.1.9) implies, for instance, that $\chi^o_{yy}(\omega = 0) = 1/\mathcal{J}(\mathbf{Q})$. This result is quite general and may be derived directly from (6.1.5); the addition of a small rotating field h_y in the y-direction, perpendicular to the exchange field, only has the consequence that the direction of the angular momentum is rotated through the angle ϕ, where $\tan\phi = h_y/h_{\mathrm{ex}}$, and hence $\delta\langle J_y\rangle = \langle J_z\rangle \tan\phi = \{1/\mathcal{J}(\mathbf{Q})\}\, h_y$. Substituting (6.1.9) with $A = B$ into (6.1.8), we obtain

$$\chi_{xx}(\mathbf{q},\omega) = \langle J_z\rangle \frac{A_{\mathbf{q}} - B_{\mathbf{q}}}{E_{\mathbf{q}}^2 - (\hbar\omega)^2} \qquad ; \quad \chi_{yy}(\mathbf{q},\omega) = \langle J_z\rangle \frac{A_{\mathbf{q}} + B_{\mathbf{q}}}{E_{\mathbf{q}}^2 - (\hbar\omega)^2}, \tag{6.1.10a}$$

with

$$E_{\mathbf{q}} = \left[A_{\mathbf{q}}^2 - B_{\mathbf{q}}^2\right]^{1/2} \tag{6.1.10b}$$

and

$$\begin{aligned} A_{\mathbf{q}} + B_{\mathbf{q}} &= 2A + \langle J_z\rangle \{\mathcal{J}(\mathbf{Q}) - \mathcal{J}(\mathbf{q})\} \\ A_{\mathbf{q}} - B_{\mathbf{q}} &= \langle J_z\rangle \left\{\mathcal{J}(\mathbf{Q}) - \tfrac{1}{2}\mathcal{J}(\mathbf{q}+\mathbf{Q}) - \tfrac{1}{2}\mathcal{J}(\mathbf{q}-\mathbf{Q})\right\}, \end{aligned} \tag{6.1.10c}$$

neglecting $\chi^o_{zz}(0)$. The absorptive components of $\overline{\overline{\chi}}_t(\mathbf{q},\omega)$ are

$$\begin{aligned} \chi''_{xx}(\mathbf{q},\omega) &= \frac{\pi}{2}\langle J_z\rangle \left(\frac{A_{\mathbf{q}} - B_{\mathbf{q}}}{A_{\mathbf{q}} + B_{\mathbf{q}}}\right)^{\frac{1}{2}} \{\,\delta(E_{\mathbf{q}} - \hbar\omega) - \delta(E_{\mathbf{q}} + \hbar\omega)\} \\ \chi''_{yy}(\mathbf{q},\omega) &= \frac{\pi}{2}\langle J_z\rangle \left(\frac{A_{\mathbf{q}} + B_{\mathbf{q}}}{A_{\mathbf{q}} - B_{\mathbf{q}}}\right)^{\frac{1}{2}} \{\,\delta(E_{\mathbf{q}} - \hbar\omega) - \delta(E_{\mathbf{q}} + \hbar\omega)\}, \end{aligned} \tag{6.1.11}$$

demonstrating that the scattered intensities due to the two components are different, if $B_{\mathbf{q}}$ is non-zero. The neutron cross-section $d^2\sigma/dEd\Omega$, (4.2.2), is proportional to

$$\sum_{\alpha\beta}(\delta_{\alpha\beta} - \hat{\kappa}_\alpha\hat{\kappa}_\beta)\chi''_{\alpha\beta}(\boldsymbol{\kappa},\omega) = (1 - \hat{\kappa}_\zeta^2)\chi''_{\zeta\zeta}(\boldsymbol{\kappa},\omega) + (1 + \hat{\kappa}_\zeta^2)\chi''_{\eta\eta}(\boldsymbol{\kappa},\omega), \tag{6.1.12a}$$

since the $\xi\xi$- and $\eta\eta$-components are equal. The components in this equation are derived from the equality $\overline{\overline{\chi}}_t(\boldsymbol{\kappa},\omega) = \overline{\overline{\chi}}_t(\boldsymbol{\kappa}+\boldsymbol{\tau},\omega)$, and

$$\chi_{\xi\xi}(\boldsymbol{\kappa},\omega) = \chi_{\eta\eta}(\boldsymbol{\kappa},\omega) = \frac{1}{4}\left\{\chi_{yy}(\boldsymbol{\kappa}-\mathbf{Q},\omega) + \chi_{yy}(\boldsymbol{\kappa}+\mathbf{Q},\omega)\right\}$$
$$\chi_{\zeta\zeta}(\boldsymbol{\kappa},\omega) = \chi_{xx}(\boldsymbol{\kappa},\omega). \qquad (6.1.12b)$$

From this we deduce that, if the scattering vector is along the ζ-axis, we expect to observe both the spin waves propagating parallel to $\mathbf{Q}$, emerging from the magnetic Bragg peak at $\boldsymbol{\tau}+\mathbf{Q}$, and the spin waves propagating antiparallel to $-\mathbf{Q}$, but with their $\mathbf{q}$-vector determined relative to the Bragg peak at $\boldsymbol{\tau}-\mathbf{Q}$.

If $\langle J_z\rangle$ is zero, the system described by the Hamiltonian (6.1.4) is invariant with respect to a uniform rotation of all the angular momenta around the x- or ζ-axis, corresponding to the condition $[\,\sum_i J_{ix}\,,\,\mathcal{H}\,]=0$. In the helical phase, this commutation relation is unchanged, but nevertheless the system is no longer invariant with respect to such a rotation, since it will alter the phase constant φ in (6.1.1). This system is thus an example of a situation where a *continuous symmetry* is spontaneously *broken*. In this case, a theorem of Goldstone (1961) predicts the existence of collective modes with energies approaching zero as their lifetimes go to infinity. A detailed discussion of this phenomenon is given by Forster (1975). The *Goldstone mode*, or the *broken-symmetry mode*, in the helix is the spin-wave excitation occurring in $\overline{\overline{\chi}}_t(\mathbf{q},\omega)$ in the limit of $\mathbf{q}\to\mathbf{0}$. Since this mode is related to a uniform change of the phase φ, it is also called the *phason*. In the long-wavelength limit, $A_{\mathbf{q}} - B_{\mathbf{q}} \simeq \frac{1}{2}\langle J_z\rangle(\mathbf{q}\cdot\nabla)^2\mathcal{J}(\mathbf{0})$ goes to zero, and the spin wave energies $E_{\mathbf{q}} \simeq \{\frac{1}{2}(A_{\mathbf{0}}+B_{\mathbf{0}})\langle J_z\rangle(\mathbf{q}\cdot\nabla)^2\mathcal{J}(\mathbf{0})\}^{1/2}$ vanish linearly with q. The result (6.1.8) is valid in general at long wavelengths, independently of $\chi^o_{zz}(\omega)$, because the J_z-response is only mixed with the spin-wave response proportionally to $|\mathcal{J}_{yz}(\mathbf{q})|^2 \propto q^6$ in the limit of small q. In the static limit, $\chi^o_{xy}(\omega\to 0)$ vanishes by symmetry, and (6.1.8) then predicts that, in general,

$$\chi_{yy}(\mathbf{q},0) = 1/\left\{\mathcal{J}(\mathbf{Q}) - \tfrac{1}{2}\mathcal{J}(\mathbf{q}+\mathbf{Q}) - \tfrac{1}{2}\mathcal{J}(\mathbf{q}-\mathbf{Q})\right\} \propto q^{-2}$$

when $\mathbf{q}\to\mathbf{0}$, which is also in accordance with (6.1.10). The divergence of $\chi_{yy}(\mathbf{q}\to\mathbf{0},0)$ is easily understood, as this susceptibility component determines the response $\langle J_y\rangle$ to the application of a constant rotating field h_y at every site, which causes the same rotation of all the moments, corresponding to a change of the phase constant φ in (6.1.1). A rigid rotation of the helix costs no energy, and the lack of restoring forces implies that the susceptibility diverges. A divergence in the static susceptibility is not sufficient to guarantee the presence of a *soft mode* in the system, as

there might be a diffusive mode in the excitation spectrum of the diverging susceptibility component, with an intensity ($\propto \chi''(\omega)/\omega$) which goes to infinity as the critical $\mathbf{q}$ is approached. Outside the critical region, the inelastic excitation-energies must approach zero, in the absence of a diffusive mode, as a consequence of the Kramers–Kronig relation, but the excitations may be overdamped, i.e. still become diffusive, sufficiently close to the critical $\mathbf{q}$. In this case, the generator $1 - i\delta\varphi \sum_i J_{xi}$ of an infinitesimal rotation $\delta\varphi$ of the helix commutes with the Hamiltonian, and the Goldstone theorem applies, predicting that the spin waves are perfectly well-defined excitations in the limit of $\mathbf{q} \to \mathbf{0}$.

If $\mathcal{H}_\mathrm{J}$ can be neglected, the system contains one more Goldstone mode, since $\sum_i J_{i\xi}$ or $\sum_i J_{i\eta}$ now also commute with $\mathcal{H}$. The transformation $\exp(-i\theta \sum_i J_{i\xi})$ generates a tilting of the plane spanned by the moments, relative to the ξ–η plane perpendicular to $\mathbf{Q}$, giving rise to the tilted helix structure. In this configuration, the $J_{i\zeta} = J_{ix}$-component is non-zero and oscillates with the phase $\mathbf{Q}\cdot\mathbf{R}_i$. The magnitude of the modulation is determined by the susceptibility component $\chi_{xx}(\mathbf{q} = \mathbf{Q}, 0)$, which diverges in the limit where $\mathcal{H}_\mathrm{J}$ or $2A$ vanishes. The situation is very similar to the rotation of the helix considered above. The Goldstone mode is the spin-wave excitation at $\mathbf{q} = \mathbf{Q}$, and the spin-wave energy vanishes linearly with $|\mathbf{q} - \mathbf{Q}|$. The Heisenberg ferromagnet may be considered to be a helix with $\mathbf{Q} = \mathbf{0}$, and in this case the two Goldstone modes collapse into one at $\mathbf{q} = \mathbf{0}$, where the spin-wave dispersion now becomes quadratic in q.

The first study of the spin waves in a periodic magnetic structure was performed by Bjerrum Møller *et al.* (1967) on a Tb crystal, to which 10% Ho had been added to stabilize the helix over a wider temperature range. The results of these measurements are shown in Fig. 6.1. The hexagonal anisotropy in Tb is small, and $\langle O_6^6 \rangle$ has renormalized to negligible values in the helical phase, so the theory for the incommensurable structure would be expected to apply. The dispersion relations do indeed have the form of eqn (6.1.10), rising linearly from zero at small $\mathbf{q}$, and with a non-zero value of $E_\mathbf{Q}$, due to the axial anisotropy B_2^0. An analysis of the experimental results in terms of this expression gives the exchange functions illustrated in Fig. 6.1. The decrease in the size of the peak in $\mathcal{J}(\mathbf{q})$ with decreasing temperature contributes towards the destabilization of the helix, as discussed in Section 2.3. The effects of the change in this function with temperature can be seen fairly directly in the dispersion relations since, from (6.1.10), the initial slope is proportional to the square root of the curvature $\mathcal{J}''(\mathbf{Q})$, and $E_\mathbf{Q}$ is proportional to $\{\mathcal{J}(\mathbf{Q}) - \frac{1}{2}\mathcal{J}(\mathbf{0}) - \frac{1}{2}\mathcal{J}(2\mathbf{Q})\}^{1/2}$. Similar results have been obtained for Dy by Nicklow *et al.* (1971b) and analysed in the same way, even though

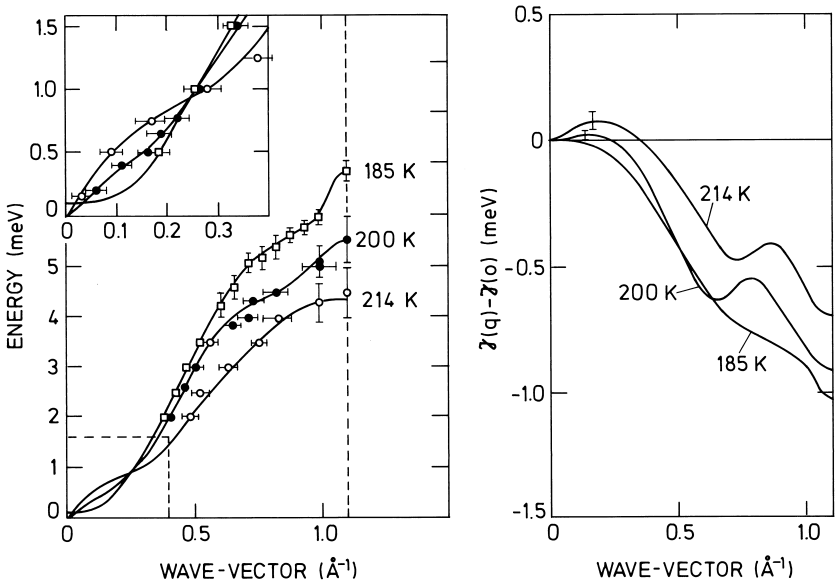

Fig. 6.1. Spin-wave dispersion relations and exchange in the c-direction, in the helical and ferromagnetic phases of $Tb_{90}Ho_{10}$. In the helical phase, the energy of the phason excitations goes linearly to zero at long wavelengths, owing to the broken rotational symmetry around the c-axis, but that of the mode at $\mathbf{Q}$ remains non-zero, because of the axial anisotropy. The peak in the exchange function, which stabilizes the periodic structure, is reduced and shifted as the magnetic order increases. In the ferromagnetic phase at 185 K, the energy rises quadratically from a non-zero value, and the peak in the exchange is absent.

the relatively large hexagonal anisotropy makes the use of this theory somewhat marginal in this case. As we shall see in the next section, the very large value of B_6^6 has a decisive influence on the excitations in Ho.

The dispersion relation for the cone may be derived by the same procedure. In the conical structure the moments along the c-axis are non-zero, so that

$$\langle J_{i\zeta}\rangle = \langle J_{\parallel}\rangle = \langle J_z\rangle \cos\theta_0 \qquad ; \quad \langle J_z\rangle^2 = \langle J_{\parallel}\rangle^2 + \langle J_{\perp}\rangle^2. \qquad (6.1.13)$$

Introducing the transformation (2.2.8), which corresponds to (6.1.3) in the case where $\cos\theta_0 \neq 0$, we may derive the effective coupling parameters within the rotating coordinate system. For the (xy)-part of the

interaction matrix, the result is

$$\begin{aligned}
\mathcal{J}_{xx}(\mathbf{q}) &= \frac{1}{2}\{\mathcal{J}(\mathbf{q}+\mathbf{Q}) + \mathcal{J}(\mathbf{q}-\mathbf{Q})\}\cos^2\theta_0 + \mathcal{J}(\mathbf{q})\sin^2\theta_0 \\
\mathcal{J}_{yy}(\mathbf{q}) &= \frac{1}{2}\{\mathcal{J}(\mathbf{q}+\mathbf{Q}) + \mathcal{J}(\mathbf{q}-\mathbf{Q})\} \\
\mathcal{J}_{xy}(\mathbf{q}) &= -\mathcal{J}_{yx}(\mathbf{q}) = \frac{i}{2}\{\mathcal{J}(\mathbf{q}+\mathbf{Q}) - \mathcal{J}(\mathbf{q}-\mathbf{Q})\}\cos\theta_0,
\end{aligned} \tag{6.1.14}$$

where $\mathcal{J}_{xy}(\mathbf{q})$ is now non-zero. Neglecting the longitudinal response, as we may in a weakly anisotropic system, we may calculate the response functions by introducing these coupling parameters in (6.1.8). In order to estimate the (xy)-components of the MF susceptibility, or $A \pm B + h_{\rm ex}$ in eqn (6.1.9), we may utilize their relation to the derivatives of the free energy, as expressed in eqn (2.2.18). The free energy for the ith ion, including the Zeeman contribution from the exchange field of the surrounding ions, is

$$F(i) = f_0 + f(u = \cos\theta) - h_{\parallel}\langle J_z\rangle\cos\theta - h_{\perp}\langle J_z\rangle\sin\theta\cos(\phi - \phi_0), \tag{6.1.15a}$$

with $\phi_0 = \mathbf{Q}\cdot\mathbf{R}_i + \varphi$, and

$$h_{\parallel} = \langle J_z\rangle\mathcal{J}(\mathbf{0})\cos\theta_0 \qquad ; \quad h_{\perp} = \langle J_z\rangle\mathcal{J}(\mathbf{Q})\sin\theta_0. \tag{6.1.15b}$$

$\mathcal{H}_{\rm J}$ is again, as in (6.1.4), the usual crystal-field Hamiltonian, except that B_6^6 is neglected. The function $f(u)$ is given by (2.2.17) in terms of $\kappa_l^m(T)$, with $\kappa_6^6 = 0$. From (6.1.15), the equilibrium angles are determined by

$$-f'(u_0)\sin\theta_0 + h_{\parallel}\langle J_z\rangle\sin\theta_0 - h_{\perp}\langle J_z\rangle\cos\theta_0 = 0,$$

and $\phi = \phi_0$. $f'(u)$ is the derivative of $f(u)$ with respect to u, and $u_0 = \cos\theta_0$. With $\sin\theta_0 \neq 0$, this equation leads to

$$f'(u_0)\cos\theta_0 = \langle J_z\rangle^2\{\mathcal{J}(\mathbf{0}) - \mathcal{J}(\mathbf{Q})\}\cos^2\theta_0. \tag{6.1.16}$$

The spin-wave parameters may then be derived as

$$\begin{aligned}
\langle J_z\rangle(A + B + h_{\rm ex}) &= F_{\theta\theta}(i) \\
&= f''(u_0)\sin^2\theta_0 - f'(u_0)\cos\theta_0 + h_{\parallel}\langle J_z\rangle\cos\theta_0 + h_{\perp}\langle J_z\rangle\sin\theta_0 \\
\langle J_z\rangle(A - B + h_{\rm ex}) &= F_{\phi\phi}(i)/\sin^2\theta_0 = h_{\perp}\langle J_z\rangle/\sin\theta_0.
\end{aligned}$$

Introducing the values of the exchange fields and applying the equilibrium condition (6.1.16), we then find that

$$\begin{aligned}
A + B + h_{\rm ex} &= \{f''(u_0)/\langle J_z\rangle\}\sin^2\theta_0 + \langle J_z\rangle\mathcal{J}(\mathbf{Q}) \\
A - B + h_{\rm ex} &= \langle J_z\rangle\mathcal{J}(\mathbf{Q}).
\end{aligned} \tag{6.1.17}$$

These parameters determine the (xy)-components of $\overline{\overline{\chi}}^{o}(\omega)$ in (6.1.9), and are valid, at least, to first order in $1/J$. From (6.1.8), we finally obtain

$$\begin{aligned}
\chi_{xx}(\mathbf{q},\omega) &= \langle J_z\rangle \frac{A_{\mathbf{q}} - B_{\mathbf{q}}}{A_{\mathbf{q}}^2 - B_{\mathbf{q}}^2 - (\hbar\omega - C_{\mathbf{q}})^2} \\
\chi_{yy}(\mathbf{q},\omega) &= \langle J_z\rangle \frac{A_{\mathbf{q}} + B_{\mathbf{q}}}{A_{\mathbf{q}}^2 - B_{\mathbf{q}}^2 - (\hbar\omega - C_{\mathbf{q}})^2} \\
\chi_{xy}(\mathbf{q},\omega) &= \langle J_z\rangle \frac{i(\hbar\omega - C_{\mathbf{q}})}{A_{\mathbf{q}}^2 - B_{\mathbf{q}}^2 - (\hbar\omega - C_{\mathbf{q}})^2},
\end{aligned} \tag{6.1.18}$$

where the parameters are now

$$\begin{aligned}
A_{\mathbf{q}} - B_{\mathbf{q}} &= \langle J_z\rangle\{\mathcal{J}(\mathbf{Q}) - \tfrac{1}{2}\mathcal{J}(\mathbf{q}+\mathbf{Q}) - \tfrac{1}{2}\mathcal{J}(\mathbf{q}-\mathbf{Q})\} \\
A_{\mathbf{q}} + B_{\mathbf{q}} &= (A_{\mathbf{q}} - B_{\mathbf{q}})\cos^2\theta_0 + \big[L + \langle J_z\rangle\{\mathcal{J}(\mathbf{0}) - \mathcal{J}(\mathbf{q})\}\big]\sin^2\theta_0 \\
C_{\mathbf{q}} &= \tfrac{1}{2}\langle J_z\rangle\{\mathcal{J}(\mathbf{q}-\mathbf{Q}) - \mathcal{J}(\mathbf{q}+\mathbf{Q})\}\cos\theta_0,
\end{aligned} \tag{6.1.19}$$

and the axial anisotropy constant is

$$\begin{aligned}
L &= \langle J_z\rangle\{\mathcal{J}(\mathbf{Q}) - \mathcal{J}(\mathbf{0})\} + f''(u_0)/\langle J_z\rangle, \qquad \text{with} \\
f''(u_0) &= 3\kappa_2^0(T) + \tfrac{15}{2}\kappa_4^0(T)(7\cos^2\theta_0 - 1) \\
&\qquad + \tfrac{105}{8}\kappa_6^0(T)(33\cos^4\theta_0 - 18\cos^2\theta_0 + 1).
\end{aligned} \tag{6.1.20}$$

This constant, to order $1/J$, is that determined by the c-axis bulk susceptibility: $\chi_{\zeta\zeta}(\mathbf{0},0) = \langle J_z\rangle/L$. The dispersion relation, derived from the pole at positive energies, is

$$E_{\mathbf{q}} = C_{\mathbf{q}} + \big[A_{\mathbf{q}}^2 - B_{\mathbf{q}}^2\big]^{1/2}, \tag{6.1.21}$$

which is no longer even with respect to $\mathbf{q}$, because the parameter $C_{\mathbf{q}}$ changes sign, whereas $A_{\mathbf{q}}$ and $B_{\mathbf{q}}$ are unaffected, if $\mathbf{q}$ is replaced by $-\mathbf{q}$. The other pole, with a minus before the square root, lies at negative energies. If the two energies for $\mathbf{q}$ were both positive, the two poles at $-\mathbf{q}$ would both lie at negative energies, indicating an instability of the magnetic system. Hence in a stable cone $C_{\mathbf{q}}^2 < A_{\mathbf{q}}^2 - B_{\mathbf{q}}^2$ (Cooper *et al.* 1962).

The scattering cross-section of the spin waves is still determined by (6.1.12*a*), but (6.1.12*b*) is replaced by

$$\begin{aligned}
\chi_{\zeta\zeta}(\boldsymbol{\kappa},\omega) &= \chi_{xx}(\boldsymbol{\kappa},\omega)\sin^2\theta_0 \\
\chi_{\xi\xi}(\boldsymbol{\kappa},\omega) = \chi_{\eta\eta}(\boldsymbol{\kappa},\omega) &= \frac{1}{4}\big\{\chi_{xx}(\boldsymbol{\kappa}-\mathbf{Q},\omega) + \chi_{xx}(\boldsymbol{\kappa}+\mathbf{Q},\omega)\big\}\cos^2\theta_0 \\
&\quad + \frac{1}{4}\big\{\chi_{yy}(\boldsymbol{\kappa}-\mathbf{Q},\omega) + \chi_{yy}(\boldsymbol{\kappa}+\mathbf{Q},\omega)\big\} \\
&\quad - \frac{i}{2}\big\{\chi_{xy}(\boldsymbol{\kappa}-\mathbf{Q},\omega) - \chi_{xy}(\boldsymbol{\kappa}+\mathbf{Q},\omega)\big\}\cos\theta_0.
\end{aligned} \tag{6.1.22}$$

When $\boldsymbol{\kappa}$ is along the c-axis, the scattering is determined by the basal-plane component alone, and introducing (6.1.18) in this expression, we find for positive energies

$$\chi''_{\xi\xi}(\boldsymbol{\kappa},\omega) = \sum_{\mathbf{q}} \frac{\pi\langle J_z\rangle}{8r_{\mathbf{q}}}\big\{(r_{\mathbf{q}}\cos\theta_0+1)^2\delta_{\mathbf{q},\boldsymbol{\kappa}-\mathbf{Q}-\boldsymbol{\tau}} + (r_{\mathbf{q}}\cos\theta_0-1)^2\delta_{\mathbf{q},\boldsymbol{\kappa}+\mathbf{Q}-\boldsymbol{\tau}}\big\}\delta(E_{\mathbf{q}}-\hbar\omega), \quad (6.1.23)$$

where the ratio $r_{\mathbf{q}} = [(A_{\mathbf{q}}-B_{\mathbf{q}})/(A_{\mathbf{q}}+B_{\mathbf{q}})]^{1/2}$. This equation is consistent with the original result of Bar'yakhtar and Maleev (1963), who also considered the spin-polarized neutron cross-section. As in the helical case, there are two branches, emerging from either of the Bragg peaks at $\boldsymbol{\tau}\pm\mathbf{Q}$, but the intensities of the two branches are no longer equal. Furthermore, the crystal will normally split up into four distinct types of domain, as the energy of the cone structure depends on the sign of neither $\cos\theta_0$ nor $Q=\mathbf{Q}\cdot\hat{\boldsymbol{\zeta}}$. The spin-wave parameter $C_{\mathbf{q}}$ changes sign with either of these two quantities, and this leads to two different values $E^+_{\mathbf{q}}$ and $E^-_{\mathbf{q}}$ of the spin-wave energies in the four domains, corresponding to regions where the signs of $\cos\theta_0$ and Q are respectively the same or different. All the vectors in (6.1.23) are along the ζ-axis, and we may therefore write the total response function at positive energies in terms of their magnitudes, in the presence of the four domains, as

$$\chi''_{\xi\xi}(\boldsymbol{\kappa},\omega) = \sum_{\mathbf{q}} \frac{\pi\langle J_z\rangle}{8r_{\mathbf{q}}}\Big[\big\{(r_{\mathbf{q}}|\cos\theta_0|+1)^2\delta_{q,\kappa-|Q|-\tau} + (r_{\mathbf{q}}|\cos\theta_0|-1)^2\delta_{q,\kappa+|Q|-\tau}\big\}\delta(E^+_{\mathbf{q}}-\hbar\omega) + \big\{(r_{\mathbf{q}}|\cos\theta_0|-1)^2\delta_{q,\kappa-|Q|-\tau} + (r_{\mathbf{q}}|\cos\theta_0|+1)^2\delta_{q,\kappa+|Q|-\tau}\big\}\delta(E^-_{\mathbf{q}}-\hbar\omega)\Big] \quad (6.1.24)$$

showing that there will normally be four spin-wave resonances in a constant-$\boldsymbol{\kappa}$ scan, at positive energies. We shall denote the spin-waves with energies determined by $E^+_{\mathbf{q}}$, when q is positive or negative respectively, as the $+q$ branch or $-q$ branch. The energy difference $E^+_{\mathbf{q}}-E^-_{\mathbf{q}} = E^+_{\mathbf{q}}-E^+_{-\mathbf{q}} = 2C^+_{\mathbf{q}}$ is normally positive, when $q=\mathbf{q}\cdot\hat{\boldsymbol{\zeta}}>0$, so that the $+q$ branch lies above the $-q$ branch. Equation (6.1.24) then predicts that neutron scans at a series of values of κ, starting from the Bragg peak at $\tau+|Q|$, will show both the $+q$ and the $-q$ branches, that the $+q$ branch will have the largest intensity when $\kappa>\tau+|Q|$, and that the response function is symmetrical around the lattice Bragg point $\kappa=\tau$. Although two of the four types of domain may be removed by the application of an external field along the c-axis, this does not remove the degeneracy with

respect to the helicity of the cone, and eqn (6.1.24) remains unchanged. Different sign conventions, stemming from whether θ_0 is determined by the ζ-component of the magnetic moments or of the angular momenta, may lead to a different labelling of the branches by $\pm q$, but this does not of course reflect any arbitrariness in, for instance, the relation between the spin-wave energies and their scattering intensities.

In Fig. 6.2 is shown the dispersion relations $E^{\pm}_{\mathbf{q}}$ obtained in the c-direction in the conical phase of Er at 4.5 K by Nicklow *et al.* (1971a). The length of the ordering wave-vector is about $\frac{5}{21}(2\pi/c)$ and the cone angle $\theta_0 \simeq 28°$. The relatively small cone angle leads to a large splitting between the $+q$ and $-q$ branches. According to the dispersion relation (6.1.21), this splitting is given by $2C_{\mathbf{q}}$, from which $\mathcal{J}(\mathbf{q})$ may readily be derived. This leaves only the axial anisotropy L as a fitting parameter in the calculation of the mean values of the spin-wave energies. This parameter may be estimated from the magnetization measurements, $L = \langle J_z \rangle / \chi_{\zeta\zeta}(\mathbf{0}, 0)$, which indicate (Jensen 1976b) that it lies between 15–25 meV. Nicklow *et al.* (1971a) were not able to derive a satisfactory account of their experimental results from the dispersion relation given by (6.1.21) in terms of $\mathcal{J}(\mathbf{q})$ and L. In order to do so, they introduced a large anisotropic coupling between the dipoles $\mathcal{J}_{\zeta\zeta}(\mathbf{q}) - \mathcal{J}(\mathbf{q})$, corresponding to a $\mathbf{q}$-dependent contribution to $L = L(\mathbf{q})$ in (6.1.19). Although this model can account for the spin-wave energies, the value of $L(\mathbf{0})$ is much too large in comparison with that estimated above. This large value of $L(\mathbf{q})$ also has the consequence that $r_{\mathbf{q}}$ becomes small, so that the scattering intensities of the $+q$ and $-q$ branches are predicted to be nearly equal, since $(r_{\mathbf{q}} \cos\theta_0 - 1)^2 \simeq (r_{\mathbf{q}} \cos\theta_0 + 1)^2$, in disagreement with the experimental observations. A more satisfactory model was later suggested by Jensen (1974), in which an alternative anisotropic two-ion coupling was considered; $K^{mm'}_{ll'}(ij)\widetilde{O}_{lm}(\mathbf{J}_i)\widetilde{O}_{l'm'}(\mathbf{J}_j) + \text{h.c.}$, as in (5.5.14), with $m = -m' = 2$. This coupling modifies the close relationship between $C_{\mathbf{q}}$ and $A_{\mathbf{q}} - B_{\mathbf{q}}$ found above in the isotropic case, and it was thereby possible to account for the spin-wave energies, as shown in Fig. 6.2, and for the intensity ratio between the two branches at most wave-vectors, since $r_{\mathbf{q}}$ is much closer to 1, when $\pi/c < q < 2\pi/c$, than in the model of Nicklow *et al.* (1971a). Finally, the value of L used in the fit ($L = 20$ meV) agrees with that estimated from the magnetization curves. The anisotropic component of the two-ion coupling derived in this way was found to be of the same order of magnitude as the isotropic component, but the contributions of this anisotropic interaction (with $l = l' = 2$) to the spin-wave energies and to the free energy are effectively multiplied by respectively the factor $\sin^2\theta_0$ and $\sin^4\theta_0$, where $\sin^2\theta_0 \simeq 0.2$ in the cone phase. It is in fact almost possible to reproduce the dispersion relations, within the experimental uncertainty, by including

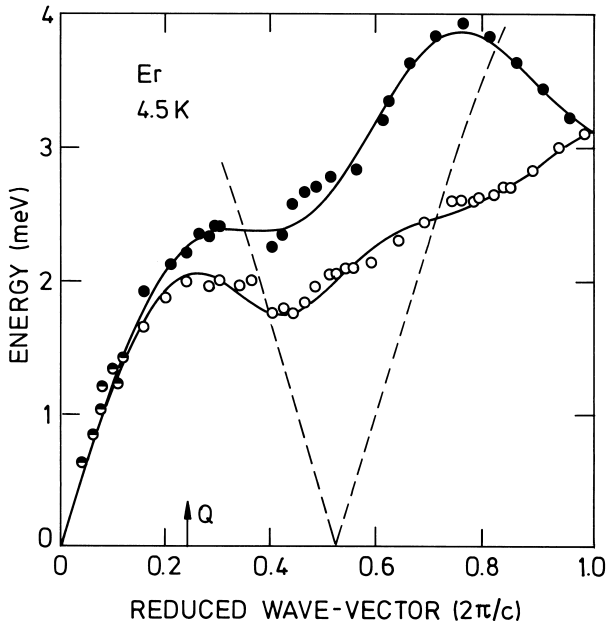

Fig. 6.2. Spin-wave dispersion relations in the c-direction, in the cone phase of Er at 4.5 K, after Nicklow *et al.* (1971a). The closed and open symbols represent the $+q$ and $-q$ branches respectively. The solid lines are the results of the spin-wave calculation described in the text, and the dashed lines are the dispersion relations for the transverse phonons originating from $2\pi/c \pm 2Q$.

only the isotropic part of the coupling, but this requires a value of $L \simeq 35$ meV, and the intensity ratio, in the interval $\pi/c < q < 2\pi/c$, is found to be wrong by a factor of three or more.

It has been suggested (Lindgård 1978) that the necessity of introducing anisotropic two-ion coupling in the description of the spin-waves in Er may be an artifact due to a breakdown of the linear spin-wave theory. As discussed in Section 5.3.2, the linear theory is not valid in strongly anisotropic systems, i.e. when the numerical value of the b-parameter is large and the length of the moments is significantly smaller than their saturation value, in the low-temperature limit. However, the model for Er presented in Section 2.3, which describes the magnetic structure as a function of temperature and magnetic field reasonably well, predicts that $\sigma(T = 0)$ is only reduced by 1–2%, and that $|b| \simeq 0.08$. The excitation spectrum in the cone phase may be derived,

in the presence of arbitrarily large anisotropy, by a numerical calculation of the MF susceptibility $\overline{\overline{\chi}}^{o}(\omega)$, as determined by the crystal-field Hamiltonian and the exchange field, given by (6.1.15*b*). In the general case, it is necessary to include the total interaction-matrix $\overline{\overline{\mathcal{J}}}(\mathbf{q})$, and not only the (xy)-part as in (6.1.14), when deriving the final susceptibility matrix (6.1.7). A numerical calculation of the excitation energies, for a model which also accounts fairly accurately for the anisotropy of Er, leads to energies which are very well described by the linear spin-wave theory (Jensen 1976c), the discrepancies being only of the order of a few per cent. The spin waves are not purely transverse, as the individual moments are calculated to precess in a plane whose normal makes an angle of about 33° with the c-axis. The relation between the difference and the sum of $E^{+}_{\mathbf{q}}$ and $E^{-}_{\mathbf{q}}$ is still found to be obeyed, when the two-ion anisotropy is neglected. The experimental results therefore attest to the importance of such anisotropy effects. Except for the tilting of the plane in which the moments precess, which is not easy to detect experimentally, the linear spin-wave theory is found to give an accurate account of the excitations at low temperatures in Er. In spite of this, it is not a good approximation to consider only the ground state and the first excited state of the MF Hamiltonian, when calculating the excitation spectrum, because 10–15% of the dispersive effects are due to the coupling between the spin waves and the higher-lying MF levels. These effects are included implicitly, to a first approximation, in the linear spin-wave theory, which gives an indication of the efficacy of the Holstein–Primakoff transformation (when J is large).

We have so far neglected the hexagonal anisotropy. In Section 2.1.3, we found that B^{6}_{6} causes a bunching of the moments about the easy axes in the plane, leading to (equal) 5th and 7th harmonics in the static modulation of the moments. The cone is distorted in an analogous way, but the hexagonal anisotropy is effectively multiplied by the factor $\sin^{6}\theta_{0} \approx 0.01$ in Er. The effects of B^{6}_{6} on the spin waves are therefore small, and may be treated by second-order perturbation theory, which predicts energy gaps in the spectrum whenever $E_{\mathbf{q}} = E_{\mathbf{q}\pm 6\mathbf{Q}}$ (for a further discussion, see Arai and Felcher, 1975). In the experimental spin-wave spectrum of Er, shown in Fig. 6.2, energy gaps are visible, but not at the positions expected from the coupling due to the hexagonal anisotropy. It seems very likely that the two gaps observed close to $q = 0.4\,(2\pi/c)$ are due to an interaction with the transverse phonons. Although the normal magnetoelastic ε-coupling, which leads to energy gaps when $E_{\mathbf{q}} = \hbar\omega_{\mathbf{q}\pm\mathbf{Q}}$, might be significant for the lower branch, the positions of both gaps agree very well with those expected from an acoustic–optical coupling, occurring when $E_{\mathbf{q}} = \hbar\omega_{\mathbf{q}\pm 2\mathbf{Q}+\mathbf{b}_3}$ (in the double-zone representation), as indicated in Fig. 6.2. Although the

two gaps are close to each other on the figure, they appear in practice on different sides of $\mathbf{q} = \mathbf{0}$, and do not interfere. This interaction is equivalent to the strong optical-magnon – acoustic-phonon coupling observed in Tb, shown in Fig. 5.6. However, in Er, it is not possible to say whether or not a non-collinear component of the spin-density wave of the polarized conduction electrons is involved, as this coupling is allowed independently of whether such a component is present or not.

6.1.2 The longitudinally polarized structure

In the helix or the cone, the magnitude of the moments is constant, and a transformation to the rotating coordinate system yields a Hamiltonian which is equivalent to that of a ferromagnet, independently of whether or not the ordering is commensurable. In the longitudinally polarized phase, the length of the moments is modulated and the magnitude of the exchange field changes from site to site. This results in a modulation of the *energies* of the MF levels, whereas in the helix or the cone, it is only the *matrix elements* of the dipole moments which change. In the commensurable case, which we shall discuss in more detail in the following section, the RPA always predicts well-defined excitations. If the magnetic ordering is incommensurable, the single-site energy levels change in a pattern which never repeats itself, introducing effectively random energy-barriers along the paths of the excitations. Hence it is not obvious whether well-defined excitations can exist in this phase (Cooper *et al.* 1962). We shall focus on the effects of incommensurable ordering by considering the simplest possible model. The single-ion anisotropy terms are neglected, but in order to confine the moments along the c-axis, the two-ion dipole coupling is assumed to be anisotropic, $\mathcal{J}_{\parallel}(\mathbf{q}) \neq \mathcal{J}_{\perp}(\mathbf{q})$. Furthermore, we assume that the temperature is so close to T_N that the tendency towards squaring-up, i.e. the higher harmonics discussed in Section 2.1.4, can be neglected, in which case

$$\langle J_{i\zeta} \rangle = \mathcal{A}_i = \mathcal{A} \cos{(\mathbf{Q} \cdot \mathbf{R}_i + \varphi)}. \tag{6.1.25}$$

The exchange field acting on the ith site is then

$$h_{i\zeta}^{\text{eff}} = \sum_j \mathcal{J}_{\parallel}(ij) \mathcal{A} \cos{(\mathbf{Q} \cdot \mathbf{R}_j + \varphi)} = \mathcal{A}_i \mathcal{J}_{\parallel}(\mathbf{Q}),$$

and the transverse component of the MF Green function is

$$g_i^o(\omega) \equiv -\chi_{+-}^o(\omega) = \frac{2\mathcal{A}_i}{\hbar\omega - \mathcal{A}_i \mathcal{J}_{\parallel}(\mathbf{Q})}, \tag{6.1.26}$$

as in Section 3.5.2. Because $\chi_{++}^o(\omega)$ and $\chi_{--}^o(\omega)$ both vanish, the site-dependent equation determining the final RPA Green function $G(ij, \omega)$,

corresponding to $g_i^o(\omega)$, may be written

$$\{\hbar\omega - \mathcal{A}_i\mathcal{J}_\parallel(\mathbf{Q})\}G(ij,\omega) = 2\mathcal{A}_i\delta_{ij} - \sum_{j'}\mathcal{A}_i\mathcal{J}_\perp(ij')G(j'j,\omega), \quad (6.1.27)$$

obtained from the RPA equation (3.5.7) by multiplying with the energy denominator in $g_i^o(\omega)$. We introduce the Fourier transforms

$$G_n(\mathbf{q},\omega) = \frac{1}{N}\sum_{ij} G(ij,\omega)e^{-i\mathbf{q}\cdot(\mathbf{R}_i-\mathbf{R}_j)}e^{-in\mathbf{Q}\cdot\mathbf{R}_i}, \quad (6.1.28)$$

where n is an integer, and the coupling parameter

$$\gamma_n(\mathbf{q}) = -\tfrac{1}{2}\,\mathcal{A}\{\mathcal{J}_\parallel(\mathbf{Q}) - \mathcal{J}_\perp(\mathbf{q}+n\mathbf{Q})\}, \quad (6.1.29)$$

which is always negative ($\mathcal{A} > 0$), as the stability of the structure requires $J_\parallel(\mathbf{Q}) - \mathcal{J}_\perp(\mathbf{Q}) > 0$. From (6.1.27), we then obtain the infinite set of equations

$$\hbar\omega G_n(\mathbf{q},\omega)+\gamma_{n+1}(\mathbf{q})G_{n+1}(\mathbf{q},\omega)+\gamma_{n-1}(\mathbf{q})G_{n-1}(\mathbf{q},\omega) = \mathcal{A}(\delta_{n,1}+\delta_{n,-1}) \quad (6.1.30)$$

whenever $\mathbf{Q}$ is incommensurable. In a commensurable structure, for which $m\mathbf{Q} = p\boldsymbol{\tau}$, we determine $G_n(\mathbf{q},\omega) = G_{n+m}(\mathbf{q},\omega)$ by the corresponding finite set of m equations. Of the infinite number of Green functions, we wish to calculate the one with $n = 0$, as the transverse scattering function is proportional to $\mathrm{Im}\big[G_0(\mathbf{q},\omega)\big]$.

It is possible to rewrite eqn (6.1.30) so that $G_0(\mathbf{q},\omega)$ is expressed in terms of *infinite continued fractions*. In order to derive such an expression, we shall introduce the semi-infinite determinant D_n, with n positive,

$$D_n = \begin{vmatrix} \hbar\omega & \gamma_{n+1} & 0 & 0 & 0 & 0 & \cdots \\ \gamma_n & \hbar\omega & \gamma_{n+2} & 0 & 0 & 0 & \cdots \\ 0 & \gamma_{n+1} & \hbar\omega & \gamma_{n+3} & 0 & 0 & \cdots \\ 0 & 0 & \gamma_{n+2} & \hbar\omega & \gamma_{n+4} & 0 & \cdots \\ \vdots & \vdots & & \ddots & \ddots & \ddots & \end{vmatrix} \quad (6.1.31)$$

leaving out the variables $\mathbf{q}$ and ω. Expanding the determinant in terms of the first column, we have

$$D_n = \hbar\omega D_{n+1} - \gamma_n\gamma_{n+1}D_{n+2}. \quad (6.1.32)$$

When $n = 1$, eqn (6.1.30) may be written $\hbar\omega G_1 + \gamma_2 G_2 = \mathcal{A} - \gamma_0 G_0$, and the semi-infinite series of equations with $n \geq 1$ may be solved in terms of G_0 and D_n:

$$G_1 = (\mathcal{A} - \gamma_0 G_0)\frac{D_2}{D_1} = (\mathcal{A} - \gamma_0 G_0)\frac{1}{\hbar\omega - \gamma_1\gamma_2 D_3/D_2}, \tag{6.1.33}$$

utilizing (6.1.32) in the last step. In terms of the two infinite continued fractions ($n \geq 1$)

$$\begin{aligned} z_n(\mathbf{q},\omega) &= \frac{\gamma_n(\mathbf{q})}{\hbar\omega - \gamma_n(\mathbf{q}) z_{n+1}(\mathbf{q},\omega)} \\ z_{-n}(\mathbf{q},\omega) &= \frac{\gamma_{-n}(\mathbf{q})}{\hbar\omega - \gamma_{-n}(\mathbf{q}) z_{-n-1}(\mathbf{q},\omega)}, \end{aligned} \tag{6.1.34}$$

eqn (6.1.33) may be written $\gamma_1 G_1 = (\mathcal{A} - \gamma_0 G_0) z_1$, and in the same way, we have $\gamma_{-1} G_{-1} = (\mathcal{A} - \gamma_0 G_0) z_{-1}$. Introducing these expressions into (6.1.30), with $n = 0$, we finally obtain

$$G_0(\mathbf{q},\omega) = \mathcal{A}\frac{z_1(\mathbf{q},\omega) + z_{-1}(\mathbf{q},\omega)}{\gamma_0\{z_1(\mathbf{q},\omega) + z_{-1}(\mathbf{q},\omega)\} - \hbar\omega}. \tag{6.1.35}$$

A similar result was derived by Liu (1980). In this formal solution, there is no small parameter, except in the high-frequency limit, which allows a perturbative expansion of $G_0(\mathbf{q},\omega)$. The infinite continued fraction determining z_n never repeats itself, but it is always possible to find an $n = s$ such that z_s is arbitrary close to, for instance, z_1. This property may be used for determining the final response function when $\hbar\omega \to 0$. In this limit, we have from (6.1.34): $z_1 = -1/z_2 = z_3 = -1/z_4 = \cdots$ and, using $z_1 \simeq z_s$ for s even, we get $z_1 = -1/z_1$ or $z_1 = \pm i$. At $\mathbf{q} = \mathbf{0}$, we have by symmetry $z_1 = z_{-1} = \pm i$, which also has to be valid at any other $\mathbf{q}$. The correct sign in front of the i is determined from a replacement of ω by $\omega + i\epsilon$, where ϵ is an infinitesimal positive quantity or, more easily, from the property that $\mathrm{Im}\big[G_0(\mathbf{q},\omega)\big]$ should have the opposite sign to ω, i.e.

$$G(\mathbf{q},\omega \to 0) = \frac{\mathcal{A}}{\gamma_0} - i\frac{\mathcal{A}}{2\gamma_0^2}\hbar\omega. \tag{6.1.36a}$$

Since

$$\chi_{\xi\xi}(\mathbf{q},\omega) = \chi_{\eta\eta}(\mathbf{q},\omega) = -\frac{1}{4}\big\{G(\mathbf{q},\omega) + G^*(\mathbf{q},-\omega)\big\},$$

we get

$$\chi_{\xi\xi}(\mathbf{q},\omega \to 0) = \frac{1}{\mathcal{J}_\parallel(\mathbf{Q}) - \mathcal{J}_\perp(\mathbf{q})} + i\frac{\hbar\omega}{\mathcal{A}\{\mathcal{J}_\parallel(\mathbf{Q}) - \mathcal{J}_\perp(\mathbf{q})\}^2}. \tag{6.1.36b}$$

The imaginary term linear in ω implies that the correlation function (4.2.3), which is proportional to $\chi''_{\alpha\beta}(\mathbf{q},\omega)/\beta\hbar\omega$ for $\omega \to 0$, is non-zero in this limit. Hence the inelastic-scattering spectrum of the incommensurable system contains a tail down to zero frequency, with a magnitude at $\omega = 0$ proportional to T. At non-zero frequencies, eqn (6.1.35) can only be solved in special cases, such as if γ_n is independent of n, corresponding to $\mathcal{J}_\perp(\mathbf{q}) = 0$ (Liu 1980). In general, numerical methods must be applied. We may, for example, replace ω by $\omega + i\epsilon$ and, instead of considering the limit $\epsilon \to 0^+$, allow ϵ to stay small but non-zero (e.g. $\epsilon = 0.01|\,\omega\,|$). Then $G_0(\mathbf{q},\omega)$ becomes insensitive to the value of $z_{\pm n}$, if n is sufficiently large ($n > 50$). ϵ acts as a coarse-graining parameter, of the type mentioned at the beginning of this section, and any energy gaps in the spectrum, smaller than $\hbar\epsilon$, are smeared out. A more careful treatment of this problem has been given by Lantwin (1990). Solutions of eqn (6.1.35) have been presented by Ziman and Lindgård (1986), Lovesey (1988), and Lantwin (1990), for various values of $\mathbf{Q}$ and the axial anisotropy parameter $\mathcal{J}_\parallel(\mathbf{Q}) - \mathcal{J}_\perp(\mathbf{Q})$. The most important result is that the imaginary part of $G_0(\mathbf{q},\omega)/\omega$ contains a number

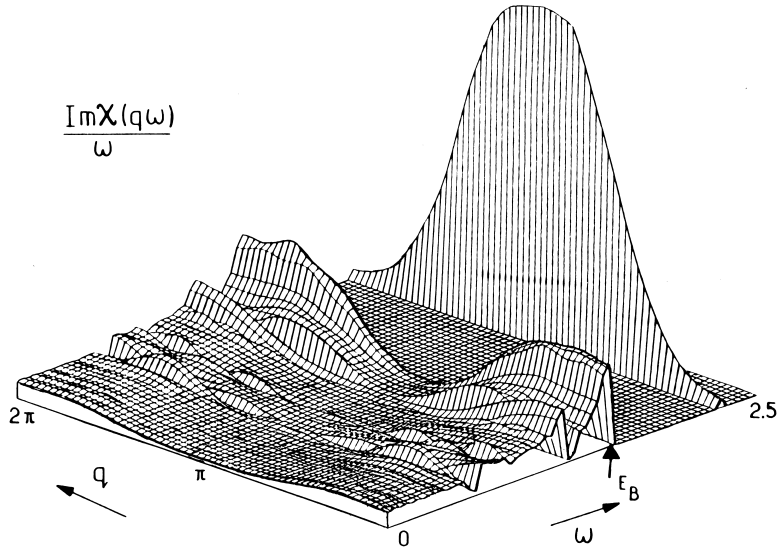

Fig. 6.3. The imaginary part of the response function $\chi_{\xi\xi}(\mathbf{q},\omega)/\omega$ for an incommensurable longitudinal structure, as a function of ω and $\mathbf{q}$, from Ziman and Lindgård (1986). The sharp peaks indicate the presence of well-defined excitations in this structure.

of sharp peaks, as a function of ω at a constant value of $\mathbf{q}$; one such example is shown in Fig. 6.3. These peaks indicate the presence of well-defined excitations. The variation of the energy with the component of $\mathbf{q}$ parallel to $\mathbf{Q}$ is very small, but the spectral weights of the different peaks change. This pattern indicates that the excitations propagating parallel to the ordering wave-vector are quasi-localized modes of composite angular momenta. This behaviour may be explained by a closer examination of the single-site response function (6.1.26). $g_i^o(\omega)$ becomes nearly zero, at non-zero frequencies, whenever $\mathcal{A}_i = \langle J_{i\zeta} \rangle$ is small, which generally occurs twice in every period. This explains the low-frequency diffusive response, and implies that the excitations become essentially trapped between the sites with small moments.

This theory may, with some modifications, be applicable to a description of Er in its high-temperature, longitudinally polarized phase ($T_N' < T < T_N$). The excitations in this temperature interval have been studied by Nicklow and Wakabayashi (1982). They found no sharp peaks in the transverse spectrum, but saw indications of relatively strong dispersive effects at small values of $\mathbf{q} \pm \mathbf{Q}$. The absence of sharp peaks in the spectrum may be explained by intrinsic linewidth effects, neglected in the RPA theory utilized above, which may be quite substantial at the relatively high temperatures of the experiments. However, the strong dispersive effects detected close to the magnetic Bragg peaks are not consistent with the results discussed above. One modification of the simple model which may be important is the squaring-up of the moments, which has been considered by Lantwin (1990). The higher harmonics lead to additional coupling terms in (6.1.30), and the analysis becomes correspondingly more complex. However, a simple argument shows that the higher harmonics result in less localized modes, and thus lead to a stronger dispersion, as also concluded by Lantwin. It is because the intervals along the c-axis in which the moments are small become narrower when the moments square up, so that the excitations may tunnel more easily through these regions. Another limitation of the theory, which may be important for Er, is that the single-site crystal-field anisotropy, neglected in the model, is probably more important than the two-ion axial anisotropy. The single-ion anisotropy splits the levels, even when the exchange field vanishes, and excited dipolar states may occur at energies suitable for allowing the excitations to propagate across sites with small moments, more freely than in the simple model. In the limit where the exchange field is small compared to the crystal-field splittings, which we shall discuss in the next chapter, the corresponding continued fractions in $G_0(\mathbf{q}, \omega)$ converge rapidly (Jensen *et al.* 1987), and the results become largely independent of whether the ordering is commensurable or not.

6.2 Commensurable periodic structures

In the preceding section, we discussed the spin-wave spectra in helical or conical systems, which are characterized by the important feature that the magnitude of the ordered moments, and hence of the exchange field, are constant. This simplification allowed an analytic derivation of the spin-wave energies, in weakly anisotropic systems. If B_6^6 only leads to a slight distortion of the structure, its effects on the spin waves may be included as a perturbation. If B_6^6 is large, however, as it is for instance in Ho, this procedure may not be sufficiently accurate. Instead it is necessary to diagonalize the MF Hamiltonian for the different sites, determine the corresponding MF susceptibilities, and thereafter solve the site-dependent RPA equation

$$\overline{\overline{\chi}}(ij,\omega) = \overline{\overline{\chi}}_i^{\,o}(\omega)\delta_{ij} + \sum_{j'} \overline{\overline{\chi}}_i^{\,o}(\omega)\overline{\overline{\mathcal{J}}}(ij')\overline{\overline{\chi}}(j'j,\omega). \tag{6.2.1}$$

In uniform para- or ferromagnetic systems, $\overline{\overline{\chi}}_i^{\,o}(\omega)$ is independent of the site considered, and the equation may be diagonalized, with respect to the site dependence, by a Fourier transformation. In an undistorted helix or cone, the transformation to the rotating coordinate system eliminates the variation of $\overline{\overline{\chi}}_i^{\,o}(\omega)$ with respect to the site index, and (6.2.1) may be solved as in the uniform case. If B_6^6 is large, the transformation to a (uniformly) rotating coordinate system leaves a residual variation in $\overline{\overline{\chi}}_i^{\,o}(\omega)$, and in the direction of the moments relative to the z-axis of the rotating coordinates. This complex situation can usually only be analysed by numerical methods. A strong hexagonal anisotropy will normally cause the magnetic structure to be commensurable with the lattice, as discussed in Section 2.3. We shall assume this condition, and denote the number of ferromagnetic hexagonal layers in one commensurable period by m, with $\mathbf{Q}$ along the c-axis. The spatial Fourier transformation of (6.2.1) then leaves m coupled equations. In order to write down these equations explicitly, we define the Fourier transforms

$$\overline{\overline{\chi}}^{\,o}(n;\omega) = \frac{1}{N}\sum_i \overline{\overline{\chi}}_i^{\,o}(\omega)\, e^{-in\mathbf{Q}\cdot\mathbf{R}_i} \tag{6.2.2a}$$

and, corresponding to (6.1.28),

$$\overline{\overline{\chi}}(n;\mathbf{q},\omega) = \frac{1}{N}\sum_{ij} \overline{\overline{\chi}}(ij,\omega)\, e^{-i\mathbf{q}\cdot(\mathbf{R}_i-\mathbf{R}_j)}\, e^{-in\mathbf{Q}\cdot\mathbf{R}_i}, \tag{6.2.2b}$$

where n is an integer. Equation (6.2.1) then leads to

$$\overline{\overline{\chi}}(n;\mathbf{q},\omega) = \overline{\overline{\chi}}^{\,o}(n;\omega) + \sum_{s=0}^{m-1} \overline{\overline{\chi}}^{\,o}(n-s;\omega)\overline{\overline{\mathcal{J}}}(\mathbf{q}+s\mathbf{Q})\overline{\overline{\chi}}(s;\mathbf{q},\omega), \tag{6.2.3}$$

where $\overline{\overline{\chi}}^{o}(n+m;\omega) = \overline{\overline{\chi}}^{o}(n;\omega)$. The m matrix equations may be solved by replacing ω by $\omega + i\epsilon$. Instead of taking the limit $\epsilon \to 0^+$, as required by the definition of the response function, ϵ is considered as non-zero but small, corresponding to a Lorentzian broadening of the excitations. Equation (6.2.3) may then be solved by a simple iterative procedure, after the diagonal term $\overline{\overline{\chi}}(n;\mathbf{q},\omega)$ has been isolated on the left-hand side of the equation. If m is not too large, and if ϵ is not chosen to be too small, this procedure is found to converge rapidly, requiring only 10–20 iterations at each $(\mathbf{q},\omega)$. The energies of the magnetic excitations at the wave-vector $\mathbf{q}$ are then derived from the position of the peaks, of width $2\hbar\epsilon$, in the calculated response function $\mathrm{Im}\big[\overline{\overline{\chi}}(0;\mathbf{q},\omega)\big]$.

The use of numerical methods, which is unavoidable in systems with complex moment-configurations, leads to less transparent results than those obtained analytically. However, compared with the linear spin-wave theory, they have the advantage that anisotropy effects may be included, even when they are large, without difficulty. The introduction of a non-zero value for ϵ means that the response function is only determined with a finite resolution, but this is not a serious drawback. The experimental results are themselves subject to a finite resolution, because of instrumental effects. Moreover, intrinsic linewidth phenomena, neglected within the RPA, provide a justification for adopting a non-zero ϵ.

The numerical method summarized above has been used for calculating the spin-wave energies in the various structures of Ho discussed in Section 2.3. In Fig. 5.9, we presented the dispersion relations in the c-direction of Ho containing 10% of Tb, in its ferromagnetic and helical phases (Larsen *et al.* 1987). The Tb content has the desirable effects of confining the moments to the basal plane, and inducing the simple bunched helix or zero-spin-slip structure (1.5.3) in the range 20–30 K, and ferromagnetism below 20 K. The commensurability of the 12-layer structure implies that the energy of the helix is no longer invariant under a uniform rotation, and an energy gap appears at long wavelengths, reflecting the force necessary to change the angle ϕ which the bunched moments make with the nearest easy axis. The excitations in this relatively straightforward structure can be treated by spin-wave theory, and the energies in the c-direction may be written in the form of eqn (6.1.10*b*):

$$E_{\mathbf{q}} = \big[A_{\mathbf{q}}^2 - B_{\mathbf{q}}^2\big]^{1/2},$$

where now

$$A_{\mathbf{q}} + B_{\mathbf{q}} = A + B + J\big\{\mathcal{J}_{\parallel}(\mathbf{0}) - \mathcal{J}_{\parallel}(\mathbf{q})\big\}, \qquad (6.2.4a)$$

and

$$A_{\mathbf{q}} - B_{\mathbf{q}} = A - B + u^2 J\{\mathcal{J}_\perp(\mathbf{Q}) - \tfrac{1}{2}\mathcal{J}_\perp(\mathbf{q}+\mathbf{Q}) - \tfrac{1}{2}\mathcal{J}_\perp(\mathbf{q}-\mathbf{Q})\}$$
$$+v^2 J\{\mathcal{J}_\perp(5\mathbf{Q}) - \tfrac{1}{2}\mathcal{J}_\perp(\mathbf{q}+5\mathbf{Q}) - \tfrac{1}{2}\mathcal{J}_\perp(\mathbf{q}-5\mathbf{Q})\}. \quad (6.2.4b)$$

In this case, the axial- and hexagonal-anisotropy terms are

$$A + B = \frac{1}{J}\{6B_2^0 J^{(2)} - 60B_4^0 J^{(4)} + 210B_6^0 J^{(6)} + 6B_6^6 J^{(6)} \cos 6\phi\}$$
$$+ J\{u^2\mathcal{J}_\perp(\mathbf{Q}) + v^2\mathcal{J}_\perp(5\mathbf{Q}) - \mathcal{J}_\parallel(\mathbf{0})\}, \quad (6.2.5a)$$

and

$$A - B = 36B_6^6 J^{(6)} \cos 6\phi, \quad (6.2.5b)$$

while u and v are determined from the bunching angle, by (1.5.3b), as respectively $\cos(\pi/12 - \phi)$ and $\sin(\pi/12 - \phi)$. As may be seen from the above expressions, the energy gap $E_{\mathbf{0}}$ in the periodic structure should be smaller than that in the ferromagnet by a factor of approximately $\cos 6\phi$, or about 0.8. The observed difference in Fig. 5.9 is considerably greater than this, and corresponds to an effective reduction of B_2^0 by about 50% in the helical phase. Such an effect can be accounted for by an anisotropic two-ion coupling of the type observed in Tb and considered in Section 5.5.2. Specifically, the term $\mathcal{C}(\mathbf{q})$ in eqn (5.5.19a) gives a contribution $\mathcal{C}(\mathbf{0})$ to $A+B$ in the ferromagnetic phase, and $\mathcal{C}(3\mathbf{Q})\cos 6\phi$ in the bunched helical structure.

As in the ferromagnetic phase, treated in Section 5.5.1, the discontinuity in the dispersion relations at $\mathbf{q} = \mathbf{0}$ is due to the classical magnetic dipole–dipole interaction. As illustrated in Fig. 5.7, the basal-plane coupling $\mathcal{J}_\perp(\mathbf{q})$ has its maximum at $\mathbf{q} \simeq \mathbf{Q}$, but the jump in the long-wavelength limit in the dipolar contribution to $\mathcal{J}_\parallel(\mathbf{q}) - \mathcal{J}_\parallel(\mathbf{0})$, which has a magnitude $4\pi g\mu_B M$ or 0.28 meV, is sufficiently large that the absolute maximum in $\mathcal{J}_\parallel(\mathbf{q})$ is shifted from $\mathbf{q} = \mathbf{Q}$ to $\mathbf{q} = \mathbf{0}$. Consequently, the soft mode, whose energy goes to zero with the vanishing of the axial anisotropy at a temperature of 20 K in pure Ho, is the long-wavelength spin wave propagating perpendicular to the c-axis, rather than the mode of wave-vector $\mathbf{Q}$ along the c-axis. As discussed in Section 2.3.1, the cone structure, rather than the tilted helix, is thereby stabilized. Near the second-order phase transition, the divergence of $\chi_{\zeta\zeta}(\mathbf{0}, 0)$ is accompanied by a vanishing of the energy gap as $(T - T_C)^{1/2}$.

The calculated small energy gap at the centre of the zone in the commensurable helix, shown in Fig. 5.9, is due to the bunching of the moments; $\varphi = \pi/2 + p\pi/3 \pm \phi$, where the sign before ϕ alternates from

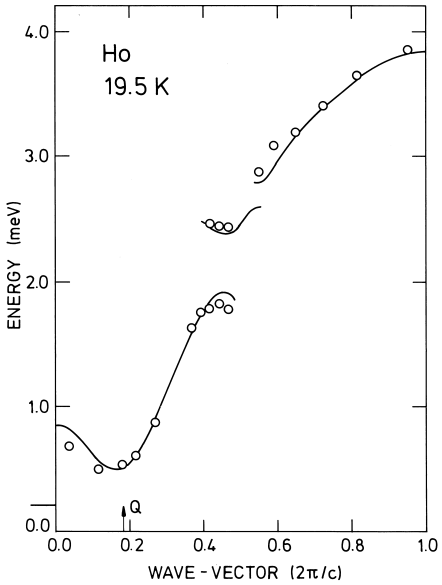

Fig. 6.4. Magnetic excitations propagating in the c-direction in the one-spin-slip structure of Ho at 20 K, after Patterson *et al.* (1990; and to be published). The full curve is the calculated dispersion relation and the points are the experimental results. The energy gap at $q = \frac{5}{11}(2\pi/c)$, due to the eleven-layer period, is resolved in these measurements. The linewidth of the scattering peaks behaves anomalously around $q = \frac{6}{11}(2\pi/c)$ suggesting a gap of the order of 0.3 meV at this wave-vector. The calculated energy of the long-wavelength modes in the basal plane is indicated by the line on the left. The discontinuity at $\mathbf{q} = \mathbf{0}$ is due to the dipolar coupling, and the transition to the cone structure is accompanied by a softening of this lowest-energy mode.

one layer to the next. This alternation doubles the periodicity in the rotating coordinate system, and thereby halves the Brillouin zone in the c-direction. The predicted gap is somewhat smaller than the experimental energy-resolution, and is therefore not observed in these measurements. The equivalent gap has however been measured in the one-spin-slip structure of Fig. 2.5 by Patterson *et al.* (1990), whose results are shown in Fig. 6.4. In this case, the 11-layer structure causes an eleven-fold reduction in the Brillouin zone, but only the first-order gap at 5/11 times $2\pi/c$ is calculated to be readily observable. This gap, on the other hand, is amplified by about a factor two, as compared to that in the structure without spin slips. As the number of spin slips increases, the calculated excitation spectra (Jensen 1988a) become more complex,

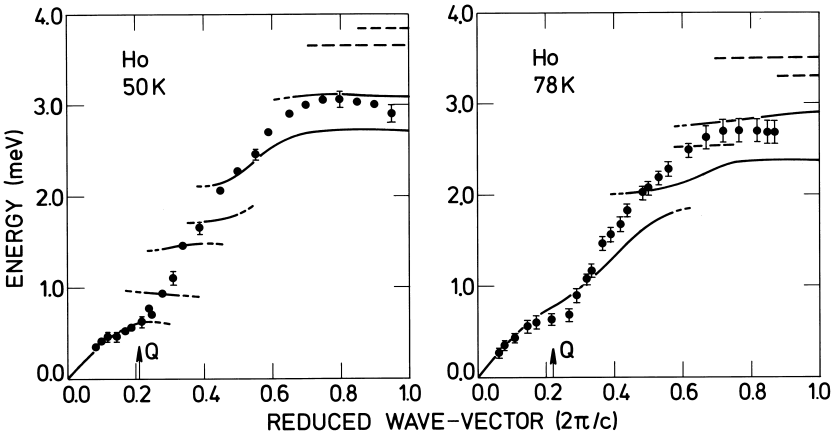

Fig. 6.5. The energies of the magnetic excitations propagating in the c-direction in the 19-layer and 9-layer spin-slip structures of Fig. 2.5. The solid lines indicate the positions of the main peaks in the calculated spectrum, whereas the dashed extensions designate peaks of relatively lower intensities. The energy gaps due to the reduced symmetry are not resolved in the experimental measurements of Nicklow (1971).

as illustrated in Fig. 6.5. The dispersion relations are broken into short segments by a succession of energy gaps, which may however be difficult to identify because of intrinsic broadening effects, neglecting in the RPA, which become more and more pronounced at increasing temperatures.

At temperatures above about 50 K, when $\langle O_6^6 \rangle$ in Ho is small and the distortion of the helix correspondingly weak, the large B_6^6 still plays an important role in mixing $|J_z>$ molecular-field (MF) states. Indeed, as the temperature is increased and the exchange field decreases, this effect becomes relatively more important, so that, for example, the energy difference between the two lowest MF levels varies by an order of magnitude as the moment on the site moves from an easy to a hard direction at elevated temperatures, while this variation is much smaller in the low-temperature limit. The large changes in the MF states from site to site tend to disrupt the coherent propagation of the collective modes, providing a mechanism for the creation of energy gaps in the excitation spectrum. The spectrum thus becomes similar to that of the incommensurable longitudinal phase, illustrated in Fig. 6.3.

Whenever the moments are not along a direction of high symmetry, B_6^6 mixes the transverse and longitudinal components of the single-site susceptibility, so that the normal modes are no longer either pure transverse spin waves or longitudinal excitations. At low temperatures, where

$\langle J_z \rangle$ is close to its maximum value, this mixing is unimportant, but it has significant effects on the excitations at higher temperatures. In the RPA, the pure longitudinal response contains an elastic component, and the (mixed) excitation spectrum in the long-wavelength limit therefore comprises an elastic and an inelastic branch. The inelastic mode is calculated to lie around 1 meV in the temperature interval 50–80 K. In the RPA, this feature is independent of whether the magnetic periodicity is commensurable with the lattice. In the incommensurable structure, the free energy is invariant to a rotation of the helix around the c-axis, implying that $\overline{\overline{\chi}}_t(\mathbf{q}, \omega)$ diverges in the limit $(\mathbf{q}, \omega) \to (\mathbf{0}, 0)$. However, the corresponding generator of rotations no longer commutes with the Hamiltonian, as in the regular helix, because B_6^6 is now non-zero. The divergence of $\overline{\overline{\chi}}_t(\mathbf{q}, \omega)$ is therefore not reflected in a conventional Goldstone mode, but is rather manifested in the elastic, zero-energy phason mode, which coexists with the inelastic mode. Beyond the RPA, the elastic response is smeared out into a diffusive mode of non-zero width. This broadening may essentially eliminate the inelastic phason mode, leaving only a diffusive peak centred at zero energy in the long-wavelength limit. The intensity of this peak diverges, and its nominal width goes to zero, when the magnetic Bragg reflection is approached. However, a diffusive-like inelastic response is still present at $\mathbf{q} = \mathbf{0}$, and a true inelastic mode only appears some distance away. In the calculations, the elastic *single-site* response was assumed to be broadened by about 6 meV, corresponding to the spin-wave bandwidth. This assumption gives a reasonable account of the excitations in the long-wavelength limit, suggesting that they become overdamped if the wave-vector is less than about 0.1 times $2\pi/c$. Although the inelastic phason mode is largely eliminated, the calculations suggest that a residue may be observable. The most favourable conditions for detecting it would occur in a neutron-scattering scan with a large component of the scattering vector in the basal plane at about 50 K.

Another example to which the above theory has been applied is Tm (McEwen *et al.* 1991), where the c-axis moments order below 57.5 K in a longitudinally polarized structure, which becomes commensurable around 32 K. Below this temperature, as described in Section 2.3.1, the structure is ferrimagnetic, comprising four layers with the moments parallel to the c-axis, followed by three layers with the moments in the opposite direction. Although Tm belongs to the heavy end of the rare earth series, the scaling factor for the RKKY-exchange interaction, $(g-1)^2 = 1/36$, is small, and the Néel temperature is low compared to the crystal-field energy-splittings. The crystal-field effects are therefore more important in this element than in the other heavy rare earths. The energy difference between the MF ground state and the dipolar excited

state is calculated to vary between 8.0 and 10.2 meV, while the exchange field lies between 0 and 1.8 meV. Hence the exchange field acts as a minor perturbation, and incommensurable effects above 32 K in the excitation spectrum should be unimportant. In the low-temperature limit, the magnetic excitations are spin waves; the MF ground state and the first dipolar excited state are almost pure $|\pm 6>$ and $|\pm 5>$ levels (+ or − depending on the site considered). The excitations propagating in the c-direction are found to lie between 8.5 and 10 meV (Fernandez-Baca *et al.* 1990; McEwen *et al.* 1991). The magnetic period is seven times that of the lattice, and the exchange coupling splits the spin waves into seven closely lying bands, which cannot be separated experimentally. With a finite resolution, the exchange coupling leads to a single or, at some wave-vectors, a double peak, whose shape and width change with $\mathbf{q}$. At low temperatures, a relatively strong coupling between the spin waves and the transverse phonons is observed, and when this coupling is included in the determination of the RPA response functions, by the method presented in Section 7.3.1 in the next chapter, good agreement is obtained between the calculated neutron spectra and those observed experimentally. At elevated temperatures, both below and just above T_N, other excitations between the excited crystal-field (MF) levels are observed to be important, both in the transverse and the longitudinal components of the response function, and good agreement is again found between theory and experiment. With respect to its magnetic properties, Tm is thus an exceptional member of the heavy rare earths, as it is the only one in which well-defined crystal-field excitations have been detected. Hence it provides an appropriate termination of our discussion of spin-waves, as well as a natural transition to the crystal-field systems which are the topic of the next chapter.